



The influence of clouds on radical concentrations: observations and modelling studies of HO_x during the Hill Cap Cloud Thuringia (HCCT) campaign in 2010

L. K. Whalley^{1,2}, D. Stone², I. J. George^{2,*}, S. Mertes³, D. van Pinxteren³, A. Tilgner³, H. Herrmann³, M. J. Evans^{4,5}, and D. E. Heard^{1,2}

¹National Centre for Atmospheric Science, University of Leeds, Leeds, LS2 9JT, UK

²School of Chemistry, University of Leeds, Leeds, LS2 9JT, UK

³Leibniz-Institut für Troposphärenforschung (TROPOS), Permoserstr. 15, 04318 Leipzig, Germany

⁴National Centre for Atmospheric Science, University of York, York, YO10 5DD, UK

⁵Department of Chemistry, University of York, York, YO10 5DD, UK

* now at: National Risk Management Research Laboratory, US Environmental Protection Agency, Research Triangle Park, North Carolina 27711, USA

Correspondence to: L. K. Whalley (l.k.whalley@leeds.ac.uk)

Received: 21 July 2014 – Published in Atmos. Chem. Phys. Discuss.: 15 September 2014

Revised: 24 February 2015 – Accepted: 1 March 2015 – Published: 23 March 2015

Abstract. The potential for chemistry occurring in cloud droplets to impact atmospheric composition has been known for some time. However, the lack of direct observations and uncertainty in the magnitude of these reactions led to this area being overlooked in most chemistry transport models. Here we present observations from Mt Schmücke, Germany, of the HO₂ radical made alongside a suite of cloud measurements. HO₂ concentrations were depleted in-cloud by up to 90 % with the rate of heterogeneous loss of HO₂ to clouds necessary to bring model and measurements into agreement, demonstrating a dependence on droplet surface area and pH. This provides the first observationally derived assessment for the uptake coefficient of HO₂ to cloud droplets and was found to be in good agreement with theoretically derived parameterisations. Global model simulations, including this cloud uptake, showed impacts on the oxidising capacity of the troposphere that depended critically on whether the HO₂ uptake leads to production of H₂O₂ or H₂O.

changes in transport, photolysis, wet deposition and in-cloud oxidation of sulfur. Modelling studies have shown that aqueous-phase chemistry can also significantly reduce gaseous HO₂ concentrations by heterogeneous uptake and loss into cloud droplets (Jacob, 1996; Tilgner et al., 2005; Huijnen et al., 2014). This chemistry is predicted to reduce OH and O₃ concentrations, also due to the reduction in the gas-phase concentration of HO₂. This in turn decreases the self-cleansing capacity of the atmosphere and increases the lifetime of many trace gases (Lelieveld and Crutzen, 1990), with impacts for climate and air quality. Aqueous-phase models have been developed which combine multi-phase chemistry with detailed microphysics (Tilgner et al., 2005), but there are limited experimental field data of gas-phase radical concentrations within clouds to corroborate model predictions of heterogeneous loss of radicals to cloud droplets. There have been a number of aircraft campaigns which have measured OH and HO₂ radical concentrations within clouds (Mauldin et al., 1997, 1998; Olson et al., 2004; Commane et al., 2010); often, however, simultaneous observations of cloud droplet number and size distributions (or other key gas-phase radical precursors) were not made during these studies, making it difficult to assess the full impact of clouds on radical concentrations. In general therefore climate and air

1 Introduction

Clouds occupy around 15 % of the volume of the lower troposphere and can impact atmospheric composition through

quality models do not consider this impact of clouds on atmospheric composition.

Within the literature, a wide range of uptake coefficients of HO₂ to liquid and aerosol surfaces have been considered to reproduce observed HO₂ concentrations (e.g. Sommariva et al., 2004; Haggerstone et al., 2005; Emmerson et al., 2007; Whalley et al., 2010) with often large uptake coefficients (up to 1 at times) used to reconcile model over-predictions. A wide range of uptake coefficients, not wholly consistent with each other, have been reported from laboratory studies (Abbatt et al., 2012). From measurements conducted in our laboratory, uptake probabilities of HO₂ to sub-micron aerosols were found to be less than 0.02 at room temperature (George et al., 2013) for aqueous aerosols that did not contain significant transition metal ions; similarly low uptake coefficients were derived by Thornton and Abbatt (2005). In contrast, measurements by Taketani et al. (2008) suggest higher uptakes of ~0.1 with enhancements observed with increasing relative humidity.

The uptake of HO₂ to aqueous aerosols is driven by its high solubility in water owing to its high Henry's law constant ($= 4.0 \times 10^3 \text{ M atm}^{-1}$ at 298.15 K; Hanson et al., 1992). Once in the aqueous phase, reaction between dissolved HO₂ and its conjugate base, O₂⁻, occurs rapidly. Thornton et al. (2008) have demonstrated that the solubility and reactivity of HO₂ are temperature and pH dependent and, if the well-characterised aqueous-phase reactions (Sect. 2.3 (R1–R5)) alone are representative of the heterogeneous loss processes, only small uptake coefficients would be expected at room temperature, consistent with the work by George et al. (2013) and Thornton and Abbatt (2005). The enhanced uptake coefficients reported by Taketani et al. (2008) suggest that there may be additional competing mechanisms occurring, however.

Further uncertainties arise in the literature relating to the eventual gas-phase products from these aqueous-phase reactions. The general consensus, until recently, was that these reactions would ultimately produce H₂O₂ (Jacob, 1996), but the significance of the reactions depends critically on whether this is the case or whether, instead, H₂O is produced (Macintyre and Evans, 2011). This is significant, as H₂O₂ can photolyse to return odd hydrogen (HO_x = OH + HO₂) to the gas phase, whilst cloud uptake of HO₂ to form H₂O provides a terminal sink for HO_x. Recent work by Mao et al. (2013) postulates that a catalytic mechanism involving the coupling of the transition metal ions Cu(I)/Cu(II) and Fe(II)/Fe(III) may rapidly convert HO₂ to H₂O, rather than H₂O₂ in aqueous aerosols. The concentration and availability of dissolved Fe and Cu in cloud droplets tends to be much lower than in aqueous aerosol (Jacob, 2000), with a large fraction of Cu ions present as organic complexes (Spokes et al., 1996; Nimmo and Fones, 1997), which are far less reactive towards O₂⁻ and HO₂(aq) than the free ions (Jacob, 2000), and so it is uncertain whether the mechanism put for-

ward by Mao et al. (2013) could be extended to heterogeneous processes occurring within cloud droplets.

To better understand the role of clouds and heterogeneous processes in the oxidative capacity of the troposphere, coordinated gas-phase measurements of OH and HO₂ within clouds together with aerosol–cloud microphysical measurements are needed. The Hill Cap Cloud Thuringia 2010 (HCCT-2010) campaign which took place in 2010 aimed to characterise the interaction of particulate matter and trace gases in orographic clouds. This paper presents the impact of cloud droplets on measured gas-phase OH and HO₂ and uses these observations to assess the proposed aqueous-phase mechanisms and determine the global impact of clouds on the tropospheric oxidising capacity.

2 Experimental

The HCCT-2010 campaign took place at the Thüringer Wald mountain range in central Germany during September and October 2010. The radical measurements were made from the German Weather Service (DWD) and the Federal Environmental Office (UBA) research station located close to the summit of Mt Schmücke (the highest peak in the mountain range, 937 m a.s.l., 10°46′8.5″ E, 50°39′16.5″ N). In October, the UBA station is immersed in cloud for 25 days on average (Herrmann et al., 2005) and, hence, is highly suitable for the study of gas and aerosol interactions with orographic cloud. Two additional experimental sites, approximately 4 km upwind of the summit site at Goldlauter and approximately 3 km downwind of the summit at Gelhberg, were also equipped with a number of instruments which enabled the processing of a single air parcel as it passed through a cloud to be assessed by multi-phase trajectory models such as SPACCIM (SPectral Aerosol Cloud Chemistry Interaction Model; Wolke et al., 2005; see Sect. 2.3). Further details of the locations may be found in Herrmann et al. (2005).

2.1 Radical measurements

OH and HO₂ measurements were made using the fluorescence assay by gas expansion technique (FAGE). Details of the instrumentation can be found in Whalley et al. (2010). A single FAGE fluorescence cell was used for sequential measurements of OH and HO₂. This was operated from the top of a 22 m high tower to co-locate with cloud measurements and ensure that the measurements were performed in full cloud. The cell was held at 1 Torr using a roots blower backed rotary pump system which was housed in an air-conditioned shipping container at the base of the tower (Fig. 1) and was connected to the cell via 30 m of flexible hosing (5 cm outer diameter – OD). A 308 nm tuneable, pulsed laser light was used to electronically excite OH radicals; this was delivered to the cell via a 30 m fibre optic cable (Oz optics) with the laser system (a Nd:YAG pumped Ti:Sapphire, Photonic In-

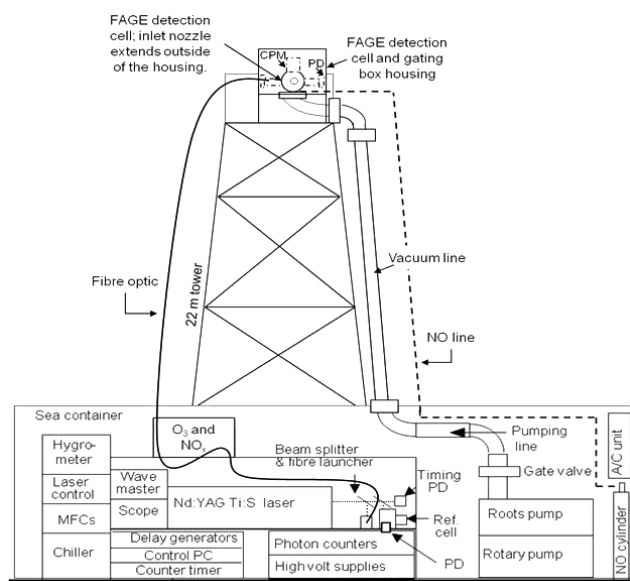


Figure 1. Schematic of the FAGE instrument set-up during the HCCT-2010 campaign. “PD” refers to photodiode, used to normalise the observed HO_2 signal to laser power.

dustries) housed in the shipping container. Fluorescence was detected by a channel photo multiplier (CPM) (Perkin Elmer) and gated photon counting. Data were acquired every second (photon counts from 5000 laser shots), with a data acquisition cycle consisting of 220 s with the laser wavelength tuned to the OH transition (NO was injected after 110 s to rapidly convert HO_2 to OH, to allow the quantification of HO_2) and 110 s tuned away from the OH transition to determine the background signal from laser scattered light.

The sensitivity of the fluorescence cell for OH and HO_2 was determined twice weekly during the measurement period through calibration using VUV photolysis of H_2O vapour in a turbulent flow of zero air (BOC, BTCA air). Calibrations were performed at relevant H_2O vapour concentrations so as to encompass the ambient H_2O vapour concentrations observed. As such, no correction for quenching of the fluorescence signal due to changing conditions was necessary. The impact of H_2O (v) on the sensitivity of this FAGE cell type (as outlined by Commane et al., 2010) has been studied by systematically varying the H_2O concentration from 500 to 10 000 ppmv, and only $\sim 10\%$ reduction in sensitivity over this range for both OH and HO_2 was observed. This reduction is entirely explained by the known quenching of fluorescence by H_2O molecules. The lamp flux was determined by N_2O actinometry (see Commane et al. (2010) for further details); this was carried out before and after the campaign and the values agreed within 21 %; the average flux was used to determine the sensitivity. The limit of detection (LOD) at a signal-to-noise ratio of one to one data acquisition cycle was $\sim 6 \times 10^5 \text{ molec cm}^{-3}$ and $\sim 8.5 \times 10^5 \text{ molecule cm}^{-3}$ for OH and HO_2 , respectively.

A number of operational modifications (from the standard University of Leeds ground-based operations; Whalley et al., 2010) were necessary to facilitate measurements of the gas-phase concentrations of the radicals within clouds. As tower measurements were required (a schematic of the measurement set-up is provided in Fig. 1), a single, smaller (4.5 cm (ID) diameter stainless steel cylinder) FAGE fluorescence cell based on the University of Leeds aircraft cell design (Commane et al., 2010) was used for sequential measurements of OH and HO_2 . Ambient air was drawn into the cell through a 1 mm diameter pinhole nozzle. The distance between sampling nozzle and radical detection region was 18 cm and NO (10 SCCM, BOC, 99.5 %) was injected ~ 8 cm below the nozzle for titration of HO_2 to OH.

The fluorescence cell was orientated with the nozzle pointing horizontal to the ground in an attempt to minimise water pooling on the nozzle and being sucked into the cell during cloud events. Occasional droplets were ingested by the cell and resulted in an instantaneous large increase in the laser scattered signal. These spiked increases were discrete and short-lived; the data presented here have been filtered to remove these spikes, which were easy to identify.

Tests have been conducted post-campaign to determine the level of HO_2 interference from RO_2 radicals (Fuchs et al., 2011). Under this particular experimental set-up, an equivalent number of ethene-derived RO_2 radicals to HO_2 were found to contribute 46 % to the total HO_2 signal (Whalley et al., 2013). The FAGE instrument was found not to be sensitive to CH_3O_2 and other short-chain alkane-derived RO_2 radicals, but is sensitive to other alkene- and aromatic-derived RO_2 radicals, with similar sensitivities to that for ethene-derived RO_2 . The instrument is also sensitive to longer-chain alkane-derived RO_2 radicals ($> \text{C}_3$), albeit to a smaller extent, as reported by Whalley et al. (2013). For this rural environment, at this time of year, however, the contribution of alkene- and aromatic-derived RO_2 radicals to the total RO_2 budget is expected to be small, as the parent VOCs for these particular RO_2 types were at low concentrations; isoprene concentrations, for example, were on average just 12.6 pptv. As a consequence of this, the resultant HO_2 interference from RO_2 radicals should also be low.

2.2 Model expression and constraints

An analytical expression has been used to predict the mean diurnal HO_2 concentrations throughout the campaign, both during cloud events and outside of cloud events. This expression was originally developed by Carslaw et al. (1999) for modelling OH, HO_2 and RO_2 radicals in the marine boundary layer and was found to agree with full Master Chemical Mechanism (MCM) model predictions for OH and HO_2 to within 20 % for daytime hours. It has since been extended further by Smith et al. (2006) to include additional HO_2 sinks, such as heterogeneous loss (k_{Loss}). The expression, given in Eq. (3), derives from the solution of simultaneous

steady-state expressions for OH and CH₃O₂ (Eq. (1) and Eq. (2) below) and includes any primary sources of HO₂ not coming from radical propagation steps such as formaldehyde photolysis:

$$[\text{OH}] = \quad (1)$$

$$\frac{2fj(\text{O}^1\text{D})[\text{O}_3] + [\text{HO}_2](k_{\text{HO}_2+\text{NO}}[\text{NO}] + k_{\text{HO}_2+\text{O}_3}[\text{O}_3])}{k_{\text{CO}+\text{OH}}[\text{CO}] + k_{\text{H}_2+\text{OH}}[\text{H}_2] + k_{\text{HCHO}+\text{OH}}[\text{HCHO}] + k_{\text{CH}_4+\text{OH}}[\text{CH}_4] + k_{\text{NO}_2+\text{OH}}[\text{NO}_2] + k_{\text{O}_3+\text{OH}}[\text{O}_3]}$$

$$[\text{CH}_3\text{O}_2] = \frac{k_{\text{CH}_4+\text{OH}}[\text{CH}_4][\text{OH}]}{k_{\text{CH}_3\text{O}_2+\text{HO}_2}[\text{HO}_2] + k_{\text{CH}_3\text{O}_2+\text{NO}}[\text{NO}]} \quad (2)$$

$$\beta[\text{HO}_2]^3 + \gamma[\text{HO}_2]^2 + \delta[\text{HO}_2] + \varepsilon = 0, \quad (3)$$

where

$$\beta = 2k_{T2}(k_{T3}B + k_{T1}A)$$

$$\gamma = 2k_{T3}k_{T2}J_1 + 2k_{T3}k_{P5}[\text{NO}]B + 2k_{T2}k_{P4}[\text{CH}_4]B + k_T[\text{NO}_2]k_{T2}B + 2Ak_{T1}k_{P5}[\text{NO}]$$

$$\delta = 2k_{T3}k_{P5}J_1[\text{NO}] + 2k_{T2}k_{P4}J_1[\text{CH}_4] + k_TJ_1[\text{NO}_2]k_{T2} + k_TB[\text{NO}_2]k_{P5}[\text{NO}] - (J_1 + J_2)Ak_{T2}$$

$$\varepsilon = J_1k_T[\text{NO}_2]k_{P5}[\text{NO}] - (J_1 + J_2)Ak_{P5}[\text{NO}],$$

where

$$J_1 = P(\text{OH}) = 2f[\text{O}_3]j(\text{O}^1\text{D})$$

(f is the fraction of O¹D) that reacts with H₂O vapour to form OH, rather than being quenched to O(³P)).

$$J_2 = 2j(\text{HCHO} \rightarrow 2\text{HO}_2)[\text{HCHO}]$$

$$A = k_{\text{CO}+\text{OH}}[\text{CO}] + k_{\text{H}_2+\text{OH}}[\text{H}_2] + k_{\text{HCHO}+\text{OH}}[\text{HCHO}] + k_{\text{CH}_4+\text{OH}}[\text{CH}_4] + k_{\text{NO}_2+\text{OH}}[\text{NO}_2] + k_{\text{O}_3+\text{OH}}[\text{O}_3]$$

$$B = k_{\text{HO}_2+\text{NO}}[\text{NO}] + k_{\text{HO}_2+\text{O}_3}[\text{O}_3] + k_{\text{loss}}$$

$$k_T = k_{\text{OH}+\text{NO}_2}k_{T1} = k_{\text{HO}_2+\text{HO}_2}k_{T2} = k_{\text{HO}_2+\text{CH}_3\text{O}_2}$$

$$k_{T3} = k_{\text{OH}+\text{HO}_2}k_{P4} = k_{\text{CH}_4+\text{OH}}$$

$$k_{P5} = k_{\text{CH}_3\text{O}_2+\text{NO}}$$

Limited CO concentration data are available from the summit site during the project, owing to instrumental problems for the first 2 weeks of measurements. An average CO concentration of 231 ppbv was used in the analytical expression to determine HO₂ concentrations, although additional model runs at + and -1σ of this average concentration (297 ppbv and 165 ppbv respectively) were also made to assess the sensitivity of the predicted HO₂ concentration to this constraint. Similarly, only discrete (non-continuous) measurements of HCHO were made during the project; an average value of 479 pptv was used as a model constraint and further model runs at + and -1σ of this average concentration (818 pptv and 139 pptv respectively) were made.

$j(\text{O}^1\text{D})$ was measured from the top of the 22 m tower, alongside the FAGE detection cell, using a 2- π filter radiometer (Bohn et al., 2008) which pointed skywards

Table 1. Details of ancillary measurements used for comparison with radical observations and cubic model constraints.

Measurement	Instrument
Liquid water content	Gerber particle volume monitor
Particle surface area (drops)	Gerber particle volume monitor
Effective drop radius	Gerber particle volume monitor
Temperature	Automatic weather station
Relative humidity	Automatic weather station
$j(\text{O}^1\text{D})$	Filter radiometer
Cloud droplet pH	Mettler 405-60 88TE-S7/120
NO _x	Chemiluminescence detector
O ₃	TEI 42c, UV absorption
CO	Thermo Electron CO analyser
HCHO	2,4-dinitrophenylhydrazine (DNPH) cartridge samples

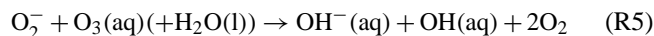
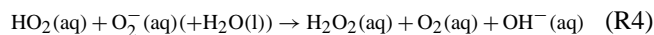
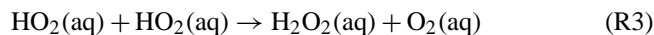
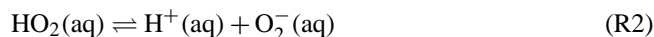
throughout the campaign. The photolysis rates of formaldehyde, $j(\text{HCHO})$, have been calculated using the Tropospheric Ultraviolet and Visible (TUV) radiation model (Madronich and Flocke, 1998). The correlation between TUV calculated $j(\text{HCHO})$ with TUV calculated $j(\text{O}^1\text{D})$ was determined, allowing these photolysis rates to be scaled to the measured $j(\text{O}^1\text{D})$ values to account for the presence of clouds. During cloud events, upward radiation will increase, with the magnitude of this increase dependent on the cloud optical depth (COD) and measurement height (Bohn, 2014). The contribution of upward radiation as a function of COD has been estimated using the TUV model using the methodology outlined by Bohn (2014). This estimated increase in upward radiation has been added to the in-cloud photolysis rates presented in Sect. 3. On average, photolysis rates are enhanced by $\sim 17\%$ during cloud events due to upwelling. A constant value of 1760 ppbv was assumed for CH₄ and a value of 508 ppbv was taken for H₂. O₃ and NO_x measurements were made from the top of the tower using commercial analysers which ran continuously from 16 September (day 3 of the field project). Details of the ancillary measurements used for comparison and model constraints are provided in Table 1. Further details of many of the measurement techniques can be found in the overview paper from an earlier hill cap cloud experiment, the Field Investigations of Budgets and Conversions of Particle Phase Organics in Tropospheric Cloud Processes (FEBUKO) project (Herrmann et al., 2005).

Rate coefficients are taken from the most recent recommendations in the Master Chemical Mechanism (MCMv3.2, <http://mcm.leeds.ac.uk/MCM/>).

A constant uptake rate for HO₂ (k_{Loss}) of 0.14 s⁻¹ to cloud droplets was included during cloud events to reproduce the average HO₂ in-cloud observations. Additional model runs with no uptake during cloud events have also been run for comparison, as have model runs in which the first-order loss to droplets was varied to replicate the HO₂ observations as a function of (i) cloud droplet surface area and (ii) pH (Sect. 3.1).

2.3 Aqueous-phase chemistry

An outline of the aqueous-phase reactions thought to be occurring, and which converts HO₂ to H₂O₂, is given below:



The equations used to calculate the theoretical increase in γ_{HO_2} with increasing pH, as proposed by Thornton et al. (2008), which have been compared with γ_{HO_2} determined in this work (Sect. 3.1), are given by

$$\frac{1}{\gamma_{\text{HO}_2}} = \frac{1}{\alpha_{\text{HO}_2}} + \frac{3\omega N_{\text{A}}}{8000(H_{\text{eff}}RT)^2 k_{\text{eff}}[\text{HO}_2(\text{g})]r_{\text{P}}}, \quad (4)$$

where

$$H_{\text{eff}} = H_{\text{HO}_2} \left[1 + \frac{K_{\text{eq}}}{[\text{H}^+]} \right] \quad (5)$$

and

$$k_{\text{eff}} = \frac{k_3 + \left(\frac{K_{\text{eq}}}{[\text{H}^+]_{\text{aq}}} \right) k_4}{\left(1 + \frac{K_{\text{eq}}}{[\text{H}^+]_{\text{aq}}} \right)^2}. \quad (6)$$

The values used in Eqs. (4)–(6) to calculate γ_{HO_2} are provided in Table 2.

2.4 Trajectory model

In addition to the modelling exercises, outlined in Sect. 2.2 above, an up-to-date chemistry process model, SPACCIM (SPectral Aerosol Cloud Chemistry Interaction Model (Wolke et al., 2005)), has been used to simulate the gas-phase HO₂ radical concentrations along a trajectory during the mountain overflow of an air parcel passing an orographic hill cap cloud to further explore the heterogeneous loss processes occurring during the cloud events encountered. This model combines complex microphysical and detailed multi-phase chemistry, permitting a detailed description of the chemical processing of gases, deliquesced particles and cloud droplets. SPACCIM incorporates the MCMv3.1-CAPRAMv4.0a mechanism (Master Chemical Mechanism (Saunders et al., 2003)/Chemical Aqueous Phase RADical Mechanism (Tilgner et al., 2013; Braeuer et al., 2015)) with 11 381 gas-phase and 7125 aqueous-phase reactions.

The MCMv3.1-CAPRAM4.0a mechanism incorporates a detailed description of the inorganic and organic multi-phase chemistry, including phase transfer in deliquesced particles and cloud droplets based on time-dependent size-resolved aerosol–cloud spectra. Further details about the SPACCIM model framework and the chemical mechanisms are given elsewhere in the literature (Tilgner et al., 2013; Wolke et al., 2005; Sehili et al., 2005, and references therein).

The measured meteorological data as well as the physical and chemical aerosol and gas-phase data at the upwind site in the village of Goldlauter provided the basis for the time-resolved initialisation of the model. In addition, separate initial box model runs with the MCM mechanism were performed to provide a more comprehensive initialisation of the chemical gas-phase composition at the simulation start. SPACCIM simulations were performed with an air parcel advected along a predefined orography – following the trajectory from the upwind site (Goldlauter) through the hill cap cloud, passing Mt Schmücke (summit site), to the downwind site (Gehlberg). Parcel simulations were performed every 20 min, allowing a time-resolved comparison of the predicted and measured HO₂ data at the summit site.

2.5 Global chemistry transport model

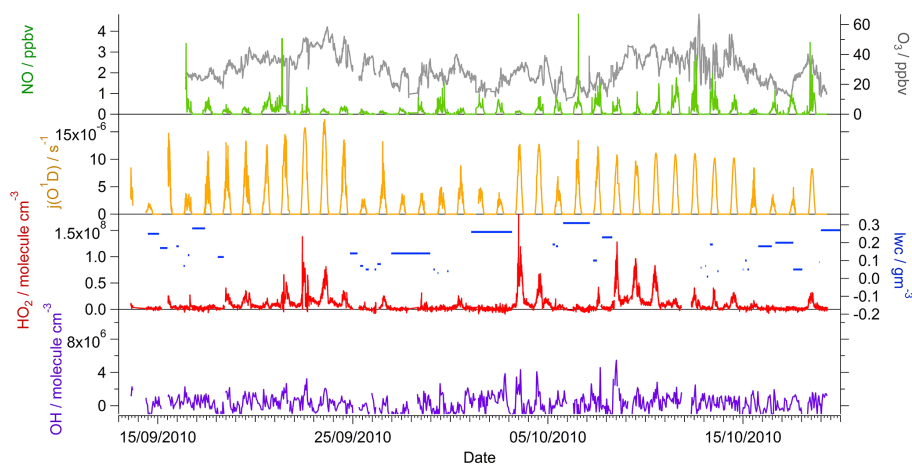
The GEOS-Chem model version 9.1.3 (www.geoschem.org) has been run to assess the global impact of the uptake of HO₂ by cloud droplets. The model was run at 2° × 2.5° global resolution for 2 years. The first year was considered a spin-up and has been ignored. The standard model includes uptake of HO₂ onto aerosols (with an uptake coefficient of 0.2), but the model has been updated in this work to include an uptake of HO₂ onto clouds. This is parameterised as a first-order loss onto clouds in a similar way to that onto aerosols following Schwartz (1984) using the temperature-dependent parameterisation of Thornton et al. (2008) with a cloud pH of 5. The cloud surface area is derived from the cloud liquid water in each model grid box (provided from the meteorological analyses) and cloud droplet radius is taken to be 6 μm over continents and 10 μm over oceans. Clouds below 258 K are assumed to be ice, and no uptake occurs. The parameterisation takes diffusional limitation in the gas phase into account, but not in the cloud phase. All simulations use the same cloud liquid water fields; thus, the impact of clouds on photolysis, wet deposition and transport is identical in all simulations.

3 Results and discussion

Near-continuous OH and HO₂ measurements were made at the Mt Schmücke site from 13 September to 19 October 2010, during which 35 separate orographic cloud events were encountered which lasted as little as 24 min to more than 2 days in duration. Figure 2 shows the time series of OH, HO₂, *j*(O¹D), NO, O₃ and liquid water content. OH con-

Table 2. The values used for the calculation of the theoretical uptake coefficient, black triangles, Fig. 5b, as a function of pH; values given at pH = 5 here.

Parameter	Value	Comments
T (Temperature)	279 K	Mean HCCT-2010 temperature
H_{HO_2} (Henry's law constant)	$1.72 \times 10^4 \text{ Matm}^{-1}$	At 279 K
H_{eff} (Effective Henry's law constant)	$8.8 \times 10^4 \text{ Matm}^{-1}$	At 279 K, pH = 5
K_{eq} (Equilibrium constant associated with R2)	$4.2 \times 10^{-5} \text{ M}$	At 279 K
k_3 (Rate constant for reaction R3)	$8.6 \times 10^5 \text{ M}^{-1} \text{ s}^{-1}$	Bielski et al. (1985)
k_4 (Rate constant for reaction R4)	$1.0 \times 10^8 \text{ M}^{-1} \text{ s}^{-1}$	Bielski et al. (1985)
k_{eff} (Effective second-order rate constant)	$1.65 \times 10^7 \text{ M}^{-1} \text{ s}^{-1}$	At 279 K, pH = 5
γ_{HO_2} (Accommodation coefficient)	1	
ω (Mean molecule speed of HO_2)	$64\,000 \text{ cm s}^{-1}$	At 279 K
N_{A} (Avogadro's number)	$6.02 \times 10^{23} \text{ mol}^{-1}$	
R (Universal gas constant)	$0.082057 \text{ atm L mol}^{-1} \text{ K}^{-1}$	
$[\text{HO}_2]$	$2 \times 10^7 \text{ molecule cm}^{-3}$	
r_{p} (Particle radius)	$6 \mu\text{m}$	Mean cloud droplet radius

**Figure 2.** Time series showing the average liquid water content during each cloud episode (blue, horizontal lines), $[\text{OH}]$ (purple), $[\text{HO}_2]$ (red), $j(\text{O}^1\text{D})$ (orange), NO (green) and O_3 (grey). All data are the average concentrations determined for each FAGE data acquisition cycle, apart from OH concentrations, which are hourly.

centrations were close to or below the limit of detection (LOD) of the instrument for much of the measurement period. A clear diurnal signal was only observable when several days of data were averaged together outside of cloud events (Fig. 3). The peak OH concentration was observed at midday at $\sim 1 \times 10^6 \text{ molecule cm}^{-3}$. No clear OH diurnal profile was observed during cloud events. HO_2 concentrations were variable, depending on whether the site was in cloud or not. The average diurnal peak concentration of HO_2 was $\sim 4 \times 10^7 \text{ molecule cm}^{-3}$ outside of cloud events (Fig. 3). A diurnal profile of HO_2 was also observed when sampling within clouds with peak concentrations reduced by approximately 90% on average. The measured rate of ozone photolysis, $j(\text{O}^1\text{D})$, varied with time of day and cloud thickness. Daily peak photolysis rates were $8.8 \times 10^{-6} \text{ s}^{-1}$

and $4.1 \times 10^{-6} \text{ s}^{-1}$ outside and within clouds, respectively. Clouds thus reduced photolysis rates by $\sim 60\%$.

Figure 4 shows the dependence of measured HO_2 concentration on cloud droplet surface area for all daytime cloud events. The observed HO_2 concentration has been divided by the observed $j(\text{O}^1\text{D})$ to remove the impact of the changing photolysis rates within the cloud. This ratio has then been normalised to 1 when the droplet surface area was zero and plotted against the cloud droplet surface area. The decrease in the ratio with increasing droplet surface area suggests that in addition to the reduction in HO_2 caused by a reduction in the photolysis rates within clouds, there is a further loss process of HO_2 that increases with cloud droplet surface area. A similar decrease in the ratio is also observed with increasing liquid water (not shown). From these observations it becomes

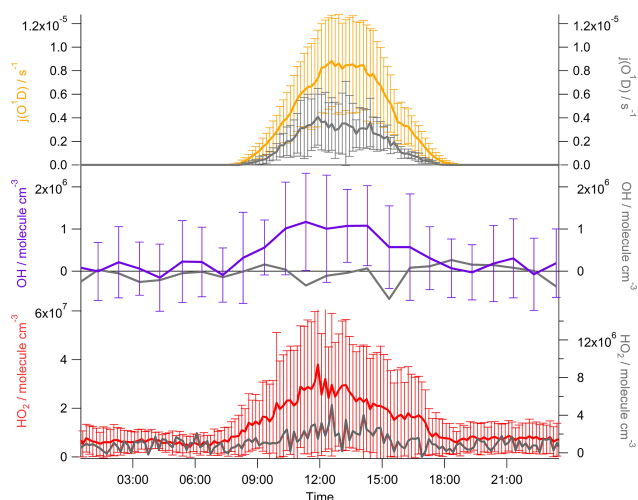


Figure 3. Average diurnal profiles of $j(\text{O}^1\text{D})$, OH and HO_2 in cloud (grey) and out of cloud (coloured). The error bars represent the 1σ variability of the averaged data; only the variability in the out-of-cloud radical data is shown for clarity. Each data point represents 10 min averaged data apart from the OH, for which the hourly averaged data are given.

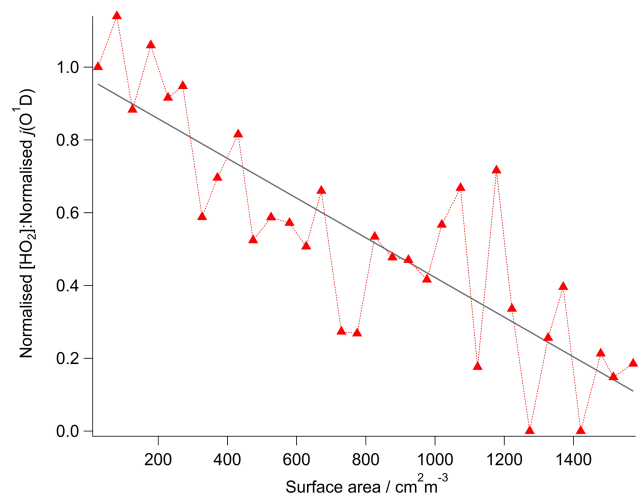


Figure 4. The dependence of the measured HO_2 concentration as a function of cloud droplet surface area. To remove the influence of changing photolysis rates, the measured HO_2 concentrations have been divided by the correspondingly observed rate of photolysis of ozone ($j(\text{O}^1\text{D})$). This ratio has then been normalised to give a value of 1 when the droplet surface area was zero. The systematic decrease in this normalised ratio with increasing droplet surface area suggests that in addition to the reduction in HO_2 caused by a reduction in the photolysis rates within clouds, there is a further loss process that increases with cloud droplet surface area. The ratio decreases linearly with increasing droplet surface area up to $1500 \text{ cm}^2 \text{ m}^{-3}$, with the line of best fit being ratio = $1 - 5 \times 10^{-4} \times \text{SA}$.

apparent that a heterogeneous process must be occurring in the presence of clouds.

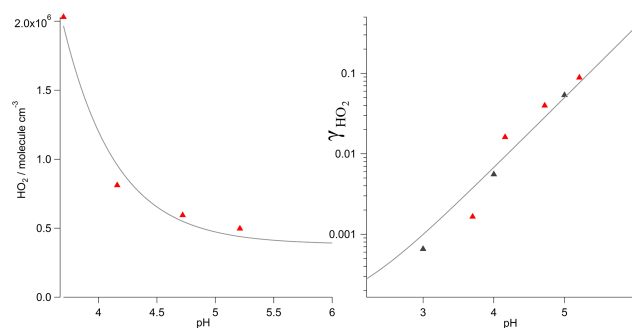


Figure 5. (a) Dependence of the HO_2 concentration observed in clouds as a function of cloud pH. All in-cloud HO_2 data were averaged into corresponding pH bins (0.6 pH units). The $[\text{HO}_2]$ decreases exponentially with increasing pH with the line of best fit ($[\text{HO}_2] = 3.8 \times 10^5 + 5.5 \times 10^9 \exp^{-2.2 \text{ pH}}$) displayed by the grey line. Figure 5b: the cloud uptake coefficient estimated by optimising the HO_2 concentration calculated from the analytic expression of Carslaw et al. (1999) compared to the observed HO_2 concentration as a function of pH (red triangles). The theoretical expression derived by Thornton et al. (2008) (Eq. 4) using parameters provided in Table 2 is shown as the black triangles with the grey line being a best-fit line for these data ($\gamma_{\text{HO}_2} = 2.15 \times 10^{-6} \exp^{2.01 \text{ pH}}$).

An insight into the mechanism by which HO_2 is lost to clouds is demonstrated by the dependence of the measured HO_2 concentration as a function of cloud water pH (Fig. 5a). Throughout the project the pH of the cloud water was recorded every hour and ranged from 3.4 to 5.3. The lowest in-cloud HO_2 occurred in clouds with the highest cloud water pH, suggesting that the solubility of HO_2 was enhanced at higher pH, as might be expected given that HO_2 is a weak acid.

3.1 Determining the uptake coefficient for HO_2 to cloud droplets

The analytical expression derived by Carslaw et al. (1999), and given in Eq. (3), has been used to estimate HO_2 concentrations both in and out of cloud events (Fig. 6). The expression represents reasonably well the campaign mean diurnal observation of HO_2 outside of the cloud events during the daytime (red dashed line and shading). During cloud events, however, the model (black dashed line and shading) overestimates the observed (grey line) HO_2 throughout the day. The inclusion of a first-order loss process ($k_{\text{Loss}} = 0.14 \text{ s}^{-1}$) in the analytical expression is able to bring the observations and calculation into better agreement on average. The cloud droplet surface area was variable during the different cloud events encountered ($1.2 \pm 0.4 \times 10^3 \text{ cm}^2 \text{ m}^{-3}$), although no diurnal trend in this parameter was evident. A clear anti-correlation between the observed HO_2 concentration and droplet surface area was observed and this correlation could only be reproduced by the analytical expression by increasing k_{Loss} in the model from $2.0 \times 10^{-2} \text{ s}^{-1}$ to $3.5 \times 10^{-1} \text{ s}^{-1}$.

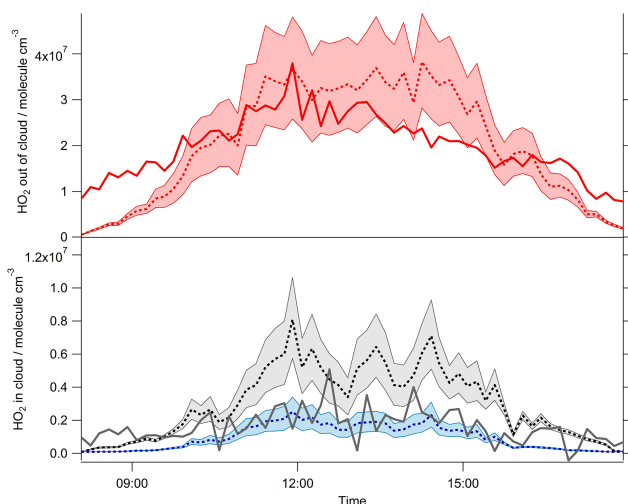


Figure 6. Upper panel. Average measured (solid red line) and simulated (dashed red line) diurnal profile of HO_2 concentrations outside of cloud events. The simulation is based on an expression originally determined by Carslaw et al. (1999) and described further in Sect. 2.2. The shading highlights the sensitivity of the model to $\pm 1\sigma$ changes in the CO and HCHO concentrations used as constraints. Lower panel. Average measured (solid grey line) and modelled (dashed black and blue lines) diurnal profile of HO_2 concentration during cloud events. The model was run without (grey) and with (blue) a loss of HO_2 to cloud droplets equal to a first-order loss rate of 0.14 s^{-1} . The shading highlights the sensitivity of the model to $\pm 1\sigma$ changes in the CO and HCHO concentrations used as constraints.

as the surface area increased from $1.2 \times 10^2 \text{ cm}^2 \text{ m}^{-3}$ to $1.5 \times 10^3 \text{ cm}^2 \text{ m}^{-3}$ (Fig. 7).

This first-order loss rate can be converted into an uptake coefficient (γ_{HO_2}) using Eq. (7) (Schwartz, 1984). Using campaign mean values for a cloud surface area (A) of $1.2 \times 10^3 \text{ cm}^2 \text{ m}^{-3}$, a droplet radius (r_p) of $6 \mu\text{m}$, a gas-phase diffusion constant for HO_2 (D_g) of $0.25 \text{ cm}^2 \text{ s}^{-1}$, and a molecular speed of HO_2 (ω) of $64\,000 \text{ cm s}^{-1}$, gives an uptake coefficient of 0.01; the uptake coefficient as a function of cloud droplet surface area is presented in the upper panel of Fig. 7.

$$k_{\text{loss}} = \left(\frac{r_p}{D_g} + \frac{4}{\gamma_{\text{HO}_2} \omega} \right)^{-1} A \quad (7)$$

These derived uptake coefficients are in good agreement with laboratory studies (Abbatt et al., 2012), including recent measurements in our laboratory, which ranged from 0.003 to 0.02, for heterogeneous loss of HO_2 on aqueous $(\text{NH}_4)_2\text{SO}_4$, NaCl and NH_4NO_3 sub-micron aerosols (George et al., 2013). This methodology provides, for the first time, a direct field assessment of the heterogeneous rate of loss of HO_2 .

Repeating this analysis but splitting the observations by cloud pH leads to values of γ_{HO_2} ranging from 1.65×10^{-3}

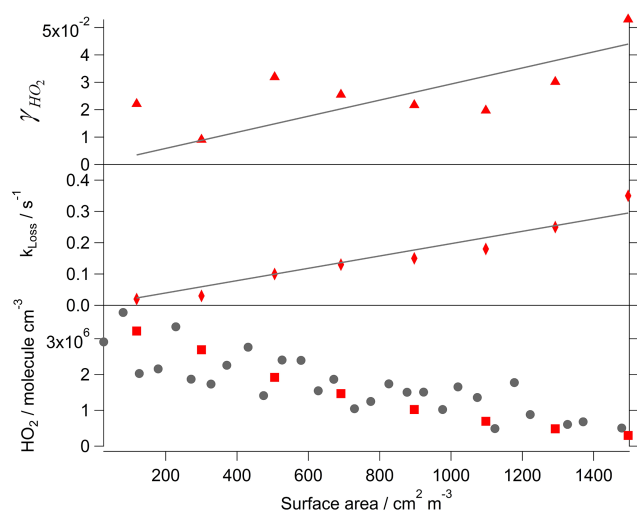


Figure 7. Lower panel. The dependence of the measured HO_2 concentration (grey circles) and modelled HO_2 concentration with a variable first-order loss (red squares) as a function of cloud droplet surface area. Middle panel. The dependence of the first-order loss term used in the model expression to best replicate the observed in-cloud HO_2 as a function cloud droplet surface area, the line of best fit being ($k_{\text{Loss}} = 2 \pm 0.1 \times 10^{-4} \times \text{SA}$). Upper panel. The dependence of γ_{HO_2} calculated using Eq. (7) as a function of cloud droplet surface area and constrained with the variable first-order loss term as shown in the middle panel. The line of best fit is ($\gamma_{\text{HO}_2} = 2.9 \pm 0.5 \times 10^{-5} \times \text{SA}$).

at a pH of 3.7 to 8.84×10^{-2} at a pH of 5.2 (Fig. 5b). These values are in good agreement with those calculated by Thornton et al. (2008), suggesting that the Thornton mechanism (which is based entirely on the known aqueous-phase chemistry) is in play in real clouds and that it can be used to estimate the heterogeneous loss of HO_2 to cloud surfaces in the troposphere.

SPACCIM simulations (Wolke et al., 2005) have also been carried out, focussing on one particular cloud event which fulfilled the required meteorological and connected flow conditions for the cloud passage experiment (additional simulations relating to the other cloud events encountered during HCCT will be presented in future publications). The modelled and measured HO_2 concentrations at Mt Schmücke during the cloud event, FCE1.1, are presented in Fig. 8. Comparisons between modelled and measured concentrations demonstrate that the simulated HO_2 concentrations are in a similar range as the measurements. The mean simulated HO_2 concentrations of $3.1 \times 10^6 \text{ molecule cm}^{-3}$ for FCE1.1 are a factor of 1.4 greater than the HO_2 measurements which were, on average, $2.2 \times 10^6 \text{ molecule cm}^{-3}$ during this particular cloud event. A further trajectory model simulation has also been run and compared to measured HO_2 concentrations at Mt Schmücke during a non-cloud event, NCE0.8. Figure 9 reveals that the model is able to reproduce the modelled HO_2 concentrations well and tracks the temporal concentration

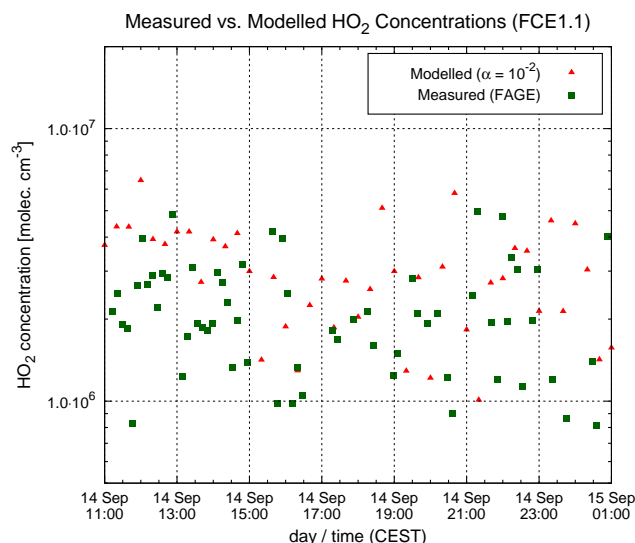


Figure 8. Comparison of the measured (green squares) and modelled (red triangles) gas-phase HO₂ concentrations at the Mt Schmücke site during cloud event FCE1.1 (14 and 15 September 2010, 11:00–01:00 CEST).

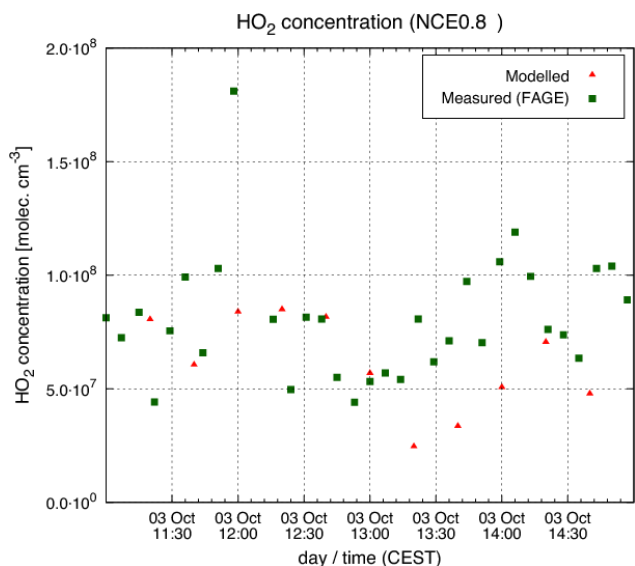


Figure 9. Comparison of the measured (green squares) and modelled (red triangles) gas-phase HO₂ concentrations at the Mt Schmücke site during non-cloud event NCE0.8.

profile throughout this event. The mean predicted HO₂ concentration is just 24 % smaller than the measurements.

The agreement between the trajectory modelled and measured in-cloud HO₂ values confirms the significant reductions in radicals within clouds predicted by complex multi-phase box models in the past (Lelieveld and Crutzen, 1990; Tilgner et al., 2005, 2013) and supports the findings presented above. Importantly, the results imply that the phase transfer data for HO₂ used within SPACCIM simulations,

e.g. the applied mass accommodation coefficient ($\alpha_{\text{HO}_2} = 10^{-2}$), are appropriate for reproducing the reduced HO₂ concentrations for in-cloud conditions. These applied parameters control the uptake fluxes towards the aqueous phase and, ultimately, the aqueous-phase HO_x levels. Confidence in the values assumed for these parameters is essential to model in-cloud oxidation within the aqueous phase accurately, with the multi-phase chemistry of other important chemical sub-systems, such as the S(IV) to S(VI) conversion, the redox cycling of transition metal ions and the processing of organic compounds all heavily dependent upon the values taken.

3.2 Global impact of the uptake of HO₂ onto cloud droplets

The GEOS-Chem (www.geos-chem.org) chemistry transport model has been used to assess the impact of the uptake of HO₂ onto cloud droplets on the global oxidising capacity using the now field-validated mechanism of Thornton et al. (2008). To investigate both the impact of the uptake and whether H₂O₂ is produced, three simulations are run, (i) with no cloud uptake of HO₂, (ii) with cloud uptake (an assumed pH of 5) of HO₂ using the Thornton mechanism to produce H₂O₂, and (iii) with cloud uptake (assumed pH of 5) of HO₂ to produce H₂O. All simulations include HO₂ uptake onto aerosol with γ_{HO_2} of 0.2, which is the standard value used in GEOS-Chem (Martin et al., 2003; Macintyre and Evans, 2011).

Figure 10 shows the annual fractional change in surface HO₂, OH, H₂O₂ and O₃ concentrations with cloud uptake switched on, and with H₂O₂ being either produced or not. Column changes are shown in Fig. 11. Both with and without H₂O₂ production, the impact is most evident in areas with long HO₂ lifetimes, i.e. regions with low NO_x and low HO₂ concentrations, and with significant cloud water densities (see Fig. 12). These are concentrated in the extra-tropics, with up to 25 and 10 % reduction in surface and column concentrations respectively. The impact on the H₂O₂ concentration depends critically on whether H₂O₂ is produced or not within clouds. In the extra-tropics there are up to 30 % increases in surface H₂O₂ if it is produced, with a similar reduction if it is not. The impacts on the surface extra-tropical oxidising capacity (OH) are of the order 10–20 % for both cases, but changes to the column values are only significant in the case where H₂O₂ is not produced. Changes in O₃ concentration are surprisingly small in both simulations. This reflects both the anti-correlation between NO concentrations and HO₂ lifetimes, and the low cloud water densities over the polluted continental regions. The largest fractional changes in HO₂ concentration occur in regions which are not producing O₃. The change in the lifetime due to the HO₂ uptake onto clouds thus has little impact on O₃ production. The large surface impact of the cloud uptake primarily reflects uptake of HO₂ by clouds at the surface (see Fig. 12a) rather than a transported impact of cloud processes from aloft

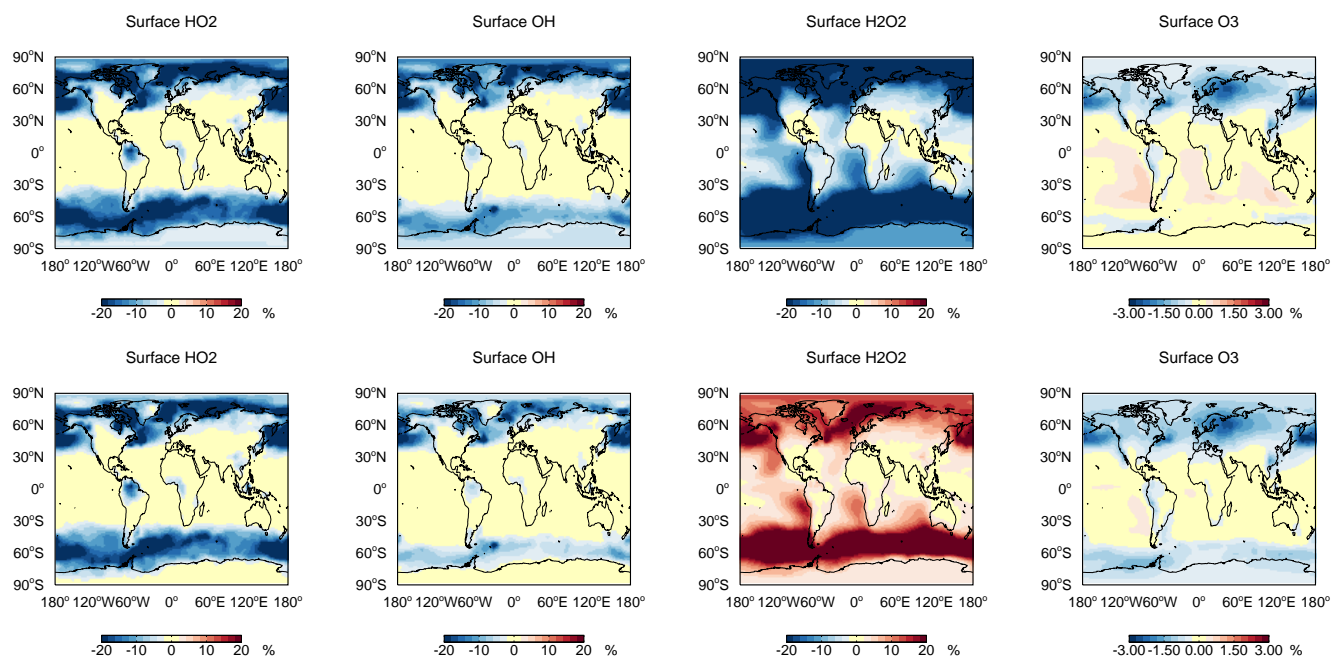


Figure 10. Annually averaged fractional change in surface HO_2 , OH , H_2O_2 and O_3 with the inclusion of HO_2 uptake into clouds leading to: (top) the production of H_2O and (bottom) the production of H_2O_2 assuming a cloud pH of 5 and the Thornton et al. (2008) parameterisation.

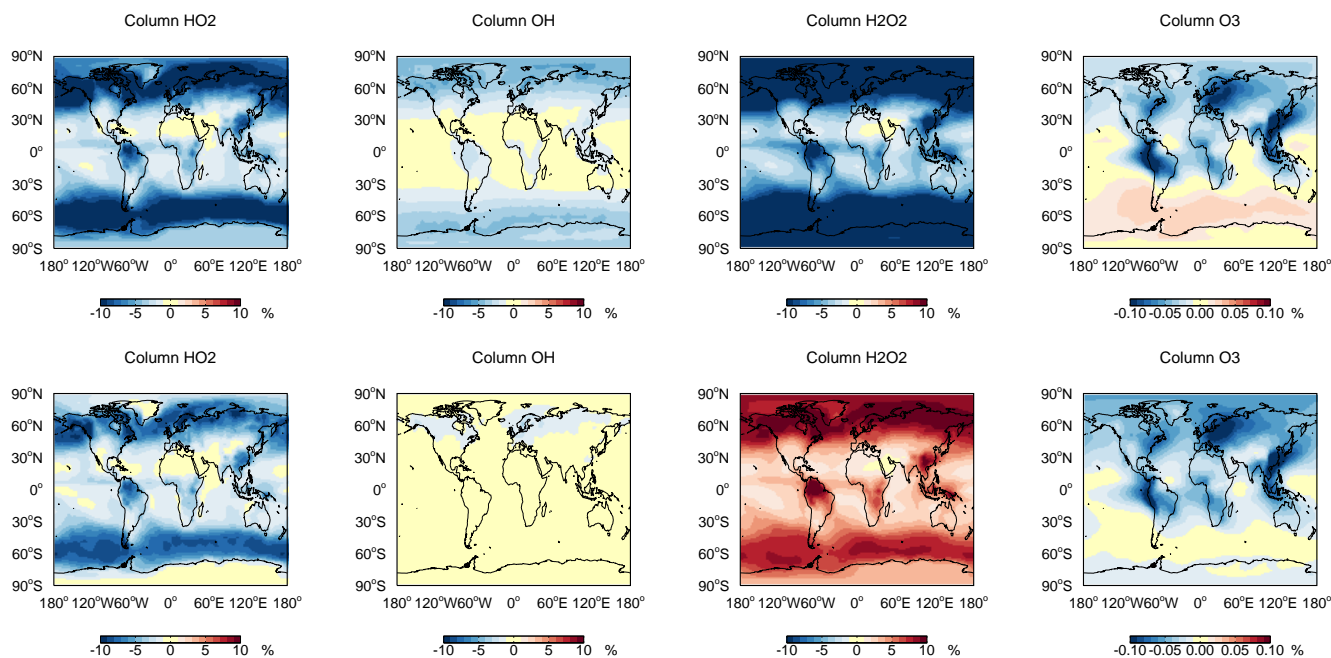


Figure 11. Annually averaged fractional change in column HO_2 , OH , H_2O_2 and O_3 with the inclusion of HO_2 uptake into clouds leading to: (top) the production of H_2O and (bottom) the production of H_2O_2 assuming a cloud pH of 5 and the Thornton et al. (2008) parameterisation.

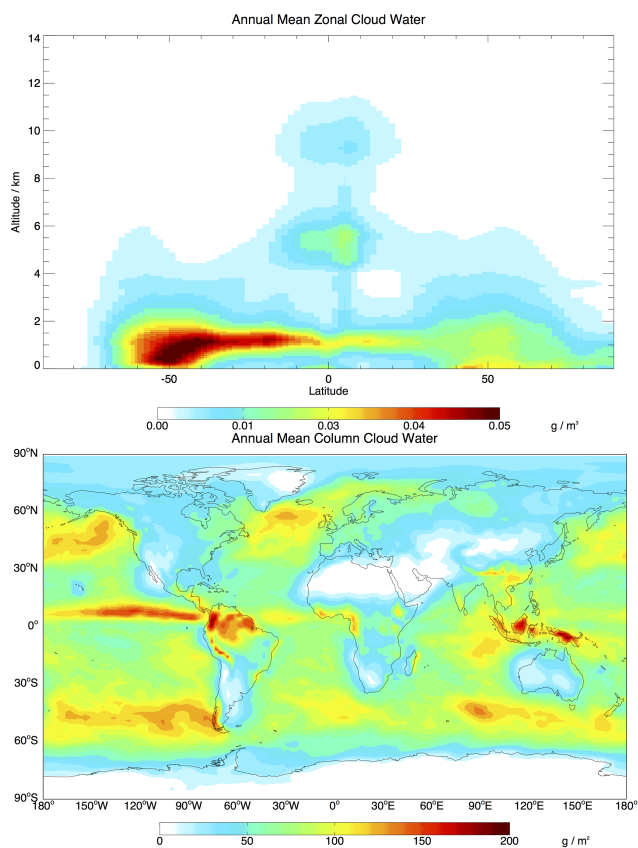


Figure 12. Annually averaged cloud water in the GEOS5 fields as (top) a column total and (bottom) a zonal mean.

downwards. The small impact on O_3 is consistent with results of Liang and Jacob (1997). These simulations make a variety of approximations as outlined in Sect. 2.5. Given the complexity of representing cloud processes occurring over the length scale of metres to hundreds of metres in a comparatively low-resolution global model (hundreds of kilometres), there are significant uncertainties as to the magnitude of these impacts. Further work in higher-resolution cloud-resolving models will be needed to estimate the full impact of these processes. Nevertheless, our observations show that the uptake of HO_2 onto clouds offers a substantial perturbation to the oxidising capacity on the local scale and that this perturbation may propagate into the regional and global scales.

4 Conclusions

We have shown here experimentally for the first time that the uptake of HO_2 onto clouds can have a significant impact on the composition of the atmosphere in a way consistent with theoretical predictions. It seems likely, however, that chemistry occurring within clouds will have other currently unknown impacts on the composition of the atmosphere. Global

and regional models need to be developed further to investigate these impacts, with predictive pH an especially important development. The impact of these processes may also change in the future with climate-induced impacts on the hydrological cycle. Further laboratory field studies and modelling are required to help resolve these remaining complex questions.

Acknowledgements. The authors would like to thank Trevor Ingham, John Spence and Matthew Broadbent for help with the development of the FAGE instrument to facilitate tower measurements. Thanks also to Birger Bohn for his useful comments on the in-cloud photolysis rates. HCCT-2010 was partially funded by the German Research Foundation (DFG), grant He 3086/15-1. Stephan Mertes' participation was funded by the DFG, grant ME-3534/1-2. Lisa Whalley, Daniel Stone, Ingrid George, Mathew Evans and Dwayne Heard are grateful to the Natural Environment Research Council for funding.

Edited by: G. McFiggans

References

- Abbatt, J. P. D., Lee, A. K. Y., and Thornton, J. A.: Quantifying trace gas uptake to tropospheric aerosol: recent advances and remaining challenges, *Chem. Soc. Rev.*, 41, 6555–6581, doi:10.1039/C2cs35052a, 2012.
- Bielski, B. H. J., Cabelli, D. E., Arudi, R. L., and Ross, A. B.: Reactivity of HO_2/O_2 radicals in aqueous solution, *J. Phys. Chem. Ref. Data*, 14, 1041–1100, doi:10.1063/1.555739, 1985.
- Bohn, B., Corlett, G. K., Gillmann, M., Sanghavi, S., Stange, G., Tensing, E., Vrekoussis, M., Bloss, W. J., Clapp, L. J., Kortner, M., Dorn, H.-P., Monks, P. S., Platt, U., Plass-Dülmer, C., Mihalopoulos, N., Heard, D. E., Clemmshaw, K. C., Meixner, F. X., Prevot, A. S. H., and Schmitt, R.: Photolysis frequency measurement techniques: results of a comparison within the ACCENT project, *Atmos. Chem. Phys.*, 8, 5373–5391, doi:10.5194/acp-8-5373-2008, 2008.
- Bohn, B.: Interactive comment on “Influence of clouds on the oxidising capacity of the troposphere” by L. K. Whalley et al., *Atmos. Chem. Phys. Discuss.*, 14, C7390–C7394, 2014.
- Brauer, P., Mouchel-Vallon, C., Tilgner, A., Mutzel, A., Böge, O., Rodigast, M., Poulain, L., van Pinxteren, D., Wolke, R., Aumont, B., and Herrmann, H.: Development of a protocol designed for the self-generation of explicit aqueous phase oxidation schemes of organic compounds, *Atmos Chem Phys Discuss.*, in preparation, 2015.
- Carslaw, N., Jacobs, P. J., and Pilling, M. J.: Modeling OH, HO_2 , and RO_2 radicals in the marine boundary layer 2. Mechanism reduction and uncertainty analysis, *J. Geophys. Res.-Atmos.*, 104, 30257–30273, doi:10.1029/1999jd900782, 1999.
- Commane, R., Floquet, C. F. A., Ingham, T., Stone, D., Evans, M. J., and Heard, D. E.: Observations of OH and HO_2 radicals over West Africa, *Atmos. Chem. Phys.*, 10, 8783–8801, doi:10.5194/acp-10-8783-2010, 2010.

- Emmerson, K. M., Carslaw, N., Carslaw, D. C., Lee, J. D., McFiggans, G., Bloss, W. J., Gravesstock, T., Heard, D. E., Hopkins, J., Ingham, T., Pilling, M. J., Smith, S. C., Jacob, M., and Monks, P. S.: Free radical modelling studies during the UK TORCH Campaign in Summer 2003, *Atmos. Chem. Phys.*, 7, 167–181, doi:10.5194/acp-7-167-2007, 2007.
- Fuchs, H., Bohn, B., Hofzumahaus, A., Holland, F., Lu, K. D., Nehr, S., Rohrer, F., and Wahner, A.: Detection of HO₂ by laser-induced fluorescence: calibration and interferences from RO₂ radicals, *Atmos. Meas. Tech.*, 4, 1209–1225, doi:10.5194/amt-4-1209-2011, 2011.
- George, I. J., Matthews, P. S. J., Whalley, L. K., Brooks, B., Goddard, A., Romero, M. T. B., and Heard, D. E.: Measurements of uptake coefficients for heterogeneous loss of HO₂ onto sub-micron inorganic salt aerosols, *Phys. Chem. Chem. Phys.*, 15, 12859–12845, 2013.
- Haggerstone, A. L., Carpenter, L. J., Carslaw, N., and McFiggans, G.: Improved model predictions of HO₂ with gas to particle mass transfer rates calculated using aerosol number size distributions, *J. Geophys. Res.-Atmos.*, 110, D04304, doi:10.1029/2004jd005282, 2005.
- Hanson, D. R., Burkholder, J. B., Howard, C. J., and Ravishankara, A. R.: Measurement of OH and HO₂ radical uptake coefficients on water and sulfuric-acid surfaces, *J. Phys. Chem.*, 96, 4979–4985, doi:10.1021/J100191a046, 1992.
- Herrmann, H., Wolke, R., Muller, K., Bruggemann, E., Gnauk, T., Barzaghi, P., Mertes, S., Lehmann, K., Massling, A., Birmili, W., Wiedensohler, A., Wierprecht, W., Acker, K., Jaeschke, W., Kramberger, H., Svrčina, B., Bachmann, K., Collett, J. L., Galgon, D., Schwirn, K., Nowak, A., van Pinxteren, D., Plewka, A., Chemnitz, R., Rud, C., Hofmann, D., Tilgner, A., Diehl, K., Heinold, B., Hinneburg, D., Knoth, O., Sehili, A. M., Simmel, M., Wurzler, S., Majdik, Z., Mauersberger, G., and Muller, F.: FEBUKO and MODMEP: field measurements and modelling of aerosol and cloud multiphase processes, *Atmos. Environ.*, 39, 4169–4183, doi:10.1016/j.atmosenv.2005.02.004, 2005.
- Huijnen, V., Williams, J. E., and Flemming, J.: Modeling global impacts of heterogeneous loss of HO₂ on cloud droplets, ice particles and aerosols, *Atmos. Chem. Phys. Discuss.*, 14, 8575–8632, doi:10.5194/acpd-14-8575-2014, 2014.
- Jacob, D. J.: Chemistry of OH in remote clouds and its role in the production of formic acid and peroxymonosulfate, *J. Geophys. Res.-Atmos.*, D9, 9807–9826, 1986.
- Jacob, D. J.: Heterogeneous chemistry and tropospheric ozone, *Atmos. Environ.*, 34, 2131–2159, doi:10.1016/S1352-2310(99)00462-8, 2000.
- Lelieveld, J. and Crutzen, P. J.: Influences of cloud photochemical processes on tropospheric ozone, *Nature*, 343, 227–233, doi:10.1038/343227a0, 1990.
- Liang, J. and Jacob, D. J.: Effect of aqueous phase cloud chemistry on tropospheric ozone, *J. Geophys. Res.-Atmos.*, 102, 5993–6001, 1997.
- Macintyre, H. L. and Evans, M. J.: Parameterisation and impact of aerosol uptake of HO₂ on a global tropospheric model, *Atmos. Chem. Phys.*, 11, 10965–10974, doi:10.5194/acp-11-10965-2011, 2011.
- Madronich, S. and Flocke, S.: The role of solar radiation in atmospheric chemistry, in: *Handbook of Environmental Chemistry*, edited by: Boule, P., Springer, New York, 1–26, 1998.
- Mao, J., Fan, S., Jacob, D. J., and Travis, K. R.: Radical loss in the atmosphere from Cu-Fe redox coupling in aerosols, *Atmos. Chem. Phys.*, 13, 509–519, doi:10.5194/acp-13-509-2013, 2013.
- Martin, R. V., Jacob, D. J., Yantosca, R. M., Chin, M., and Ginoux, P.: Global and regional decreases in tropospheric oxidants from photochemical effects of aerosols, *J. Geophys. Res.-Atmos.*, 108, 4097, doi:10.1029/2002JD0022622, 2003.
- Mauldin, R. L., Madronich, S., Flocke, S. J., Eisele, F. L., Frost, G. J., and Prevot, A. S. H.: New insights on OH: Measurements around and in clouds, *Geophys. Res. Lett.*, 24, 3033–3036, doi:10.1029/97gl02983, 1997.
- Mauldin, R. L., Frost, G. J., Chen, G., Tanner, D. J., Prevot, A. S. H., Davis, D. D., and Eisele, F. L.: OH measurements during the first Aerosol Characterization Experiment (ACE 1): observations and model comparisons, *J. Geophys. Res.-Atmos.*, 103, 16713–16729, doi:10.1029/98jd00882, 1998.
- Nimmo, M. and Fones, G. R.: The potential pool of Co, Ni, Cu, Pb and Cd organic complexing ligands in coastal and urban rain waters, *Atmos. Environ.*, 31, 693–702, doi:10.1016/S1352-2310(96)00243-9, 1997.
- Olson, J. R., Crawford, J. H., Chen, G., Fried, A., Evans, M. J., Jordan, C. E., Sandholm, S. T., Davis, D. D., Anderson, B. E., Avery, M. A., Barrick, J. D., Blake, D. R., Brune, W. H., Eisele, F. L., Flocke, F., Harder, H., Jacob, D. J., Kondo, Y., Lefer, B. L., Martinez, M., Mauldin, R. L., Sachse, G. W., Shetter, R. E., Singh, H. B., Talbot, R. W., and Tan, D.: Testing fast photochemical theory during TRACE-P based on measurements of OH, HO₂, and CH₂O, *J. Geophys. Res.-Atmos.*, 109, D15s10, doi:10.1029/2003jd004278, 2004.
- Saunders, S. M., Jenkin, M. E., Derwent, R. G., and Pilling, M. J.: Protocol for the development of the Master Chemical Mechanism, MCM v3 (Part A): tropospheric degradation of non-aromatic volatile organic compounds, *Atmos. Chem. Phys.*, 3, 161–180, doi:10.5194/acp-3-161-2003, 2003.
- Schwartz, S. E.: Gas-phase and aqueous-phase chemistry of HO₂ in liquid water clouds, *J. Geophys. Res.-Atmos.*, 89, 1589–1598, doi:10.1029/Jd089id07p11589, 1984.
- Sehili, A. M., Wolke, R., Knoth, O., Simmel, M., Tilgner, A., and Herrmann, H.: Comparison of different model approaches for the simulation of multiphase processes, *Atmos. Environ.*, 39, 4403–4417, doi:10.1016/j.atmosenv.2005.02.039, 2005.
- Smith, S. C., Lee, J. D., Bloss, W. J., Johnson, G. P., Ingham, T., and Heard, D. E.: Concentrations of OH and HO₂ radicals during NAMBLEX: measurements and steady state analysis, *Atmos. Chem. Phys.*, 6, 1435–1453, doi:10.5194/acp-6-1435-2006, 2006.
- Sommariva, R., Haggerstone, A.-L., Carpenter, L. J., Carslaw, N., Creasey, D. J., Heard, D. E., Lee, J. D., Lewis, A. C., Pilling, M. J., and Zádor, J.: OH and HO₂ chemistry in clean marine air during SOAPEX-2, *Atmos. Chem. Phys.*, 4, 839–856, doi:10.5194/acp-4-839-2004, 2004.
- Spokes, L. J., Campos, M. L. A. M., and Jickells, T. D.: The role of organic matter in controlling copper speciation in precipitation, *Atmos. Environ.*, 30, 3959–3966, doi:10.1016/1352-2310(96)00125-2, 1996.

- Taketani, F., Kanaya, Y., and Akimoto, H.: Kinetics of heterogeneous reactions of HO₂ radical at ambient concentration levels with (NH₄)₂SO₄ and NaCl aerosol particles, *J. Phys. Chem. A*, 112, 2370–2377, doi:10.1021/Jp0769936, 2008.
- Thornton, J. and Abbatt, J. P. D.: Measurements of HO₂ uptake to aqueous aerosol: mass accommodation coefficients and net reactive loss, *J. Geophys. Res.-Atmos.*, 110, D08309, doi:10.1029/2004jd005402, 2005.
- Thornton, J. A., Jaegle, L., and McNeill, V. F.: Assessing known pathways for HO₂ loss in aqueous atmospheric aerosols: regional and global impacts on tropospheric oxidants, *J. Geophys. Res.-Atmos.*, 113, D05303, doi:10.1029/2007jd009236, 2008.
- Tilgner, A., Majdik, Z., Sehili, A. M., Simmel, M., Wolke, R., and Herrmann, H.: SPACCIM: simulations of the multiphase chemistry occurring in the FEBUKO hill cap cloud experiments, *Atmos. Environ.*, 39, 4389–4401, doi:10.1016/j.atmosenv.2005.02.028, 2005.
- Tilgner, A., Brauer, P., Wolke, R., and Herrmann, H.: Modelling multiphase chemistry in deliquescent aerosols and clouds using CAPRAM3.0i, *J. Atmos. Chem.*, 70, 221–256, doi:10.1007/s10874-013-9267-4, 2013.
- Whalley, L. K., Furneaux, K. L., Goddard, A., Lee, J. D., Mahajan, A., Oetjen, H., Read, K. A., Kaaden, N., Carpenter, L. J., Lewis, A. C., Plane, J. M. C., Saltzman, E. S., Wiedensohler, A., and Heard, D. E.: The chemistry of OH and HO₂ radicals in the boundary layer over the tropical Atlantic Ocean, *Atmos. Chem. Phys.*, 10, 1555–1576, doi:10.5194/acp-10-1555-2010, 2010.
- Whalley, L. K., Blitz, M. A., Desservettaz, M., Seakins, P. W., and Heard, D. E.: Reporting the sensitivity of laser-induced fluorescence instruments used for HO₂ detection to an interference from RO₂ radicals and introducing a novel approach that enables HO₂ and certain RO₂ types to be selectively measured, *Atmos. Meas. Tech.*, 6, 3425–3440, doi:10.5194/amt-6-3425-2013, 2013.
- Wolke, R., Sehili, A. M., Simmel, M., Knoth, O., Tilgner, A., and Herrmann, H.: SPACCIM: a parcel model with detailed microphysics and complex multiphase chemistry, *Atmos. Environ.*, 39, 4375–4388, doi:10.1016/j.atmosenv.2005.02.038, 2005.